Appl. Phys. B (2014) 114:527–536
DOI 10.1007/s00340-013-5556-5

Applied Physics B
Lasers and Optics

Fermion-mediated long-range interactions between bosons stored in an optical lattice

S. De · I. B. Spielman

Received: 19 March 2013 / Accepted: 16 June 2013 / Published online: 7 July 2013

Abstract We describe a new method for creating spin-dependent long-range interactions between atomic ultra-cold neutral bosons—specifically ^{87}Rb—in an optical lattice. In this proposal, the bosonic system is immersed in a spin-polarized degenerate Fermi gas (almost perfectly non-interacting), here ^{6}Li. We first show that the bosons acquire a long-range interaction analogous to Ruderman–Kittel–Kasuya–Yosida interaction in solids. The resulting fermion-mediated Bose–Bose interaction, which can depend on the bosons' spin state, is tunable using inter-species Feshbach resonance. When the bosons are subject to a suitable optical lattice, 3-body loss processes are greatly suppressed. We conclude by showing that these interactions can lead to a supersolid phase for single-spin Bose system, and also to a fully tunable transverse field Ising model for a two-component Bose system.

1 Introduction

Ultra-cold mixtures of bosonic and fermionic atoms can realize numerous many-body Hamiltonians which may lead to better understanding of material systems. In analogy with the Cooper pairing mechanism [1] in solids, phonons in a Bose–Einstein condensate (BEC) can mediate interactions between fermions, which might help to answer open questions in Bardeen–Cooper–Schrieffer (BCS) superconductivity [2–5]. Earlier in gas mixtures of liquid Helium, the spatial dependence of the interaction between ^{3}He atoms due to exchange of ^{4}He phonons was observed [6]. Beyond the existing material systems, p-wave superfluidity of spin-polarized fermions may be induced by boson-mediated effective attractive interactions [8, 7]. The composite fermions made by pairing of fermions with bosons could generate Fermi liquid, density wave, superfluid or an insulator in an optical lattice [9]. A BEC with impurity fermions in a double-well potential has been proposed to study Josephson junction of bosons [10]. In reverse, impurity bosons embedded in a Fermi gas [11] could model interesting many-body phenomena such as the dynamics of high-T_c cuprate superconductors [12]. Going beyond material analogies, for sufficiently attractive inter-species interactions, the associated energy can overcome the Fermi pressure, leading to instabilities in degenerate Fermi gases [13]. At the unitary limit, degenerate gases could lead to understanding of stabilization processes in white dwarf and neutron stars in a well-controlled environment [14]. More practically, large Bose gases are frequently used to sympathetically cool spin-polarized Fermi gases which are otherwise non-interacting. To date, such Fermi–Bose gas mixtures include ^{6}Li–^{7}Li [15], ^{40}K–^{87}Rb [16], ^{6}Li–^{23}Na [17], ^{6}Li–^{87}Rb [18], ^{3}He* – ^{4}He* [19] and ^{171}Yb –^{174}Yb [20]. Beyond such practical applications, ultra-cold mixtures constitute a new class of many-body systems: Bosons stored in an optical lattice could exhibit exciting quantum phases such as supersolidity [21] and quantum magnetism [22] due to their long-range interactions as demonstrated here in the presence of a free spin-polarized Fermi gas.

Adding long-range interactions to cold atomic quantum gases could enable the realization of novel quantum phases

S. De (✉)
CSIR-National Physical laboratory, Dr. K. S. Krishnan Marg, New Delhi 110012, India
e-mail: subhadeep@mail.nplindia.org

I. B. Spielman
Joint Quantum Institute, National Institute of Standards and Technology, University of Maryland, Gaithersburg, MD 20899, USA

and phase transitions [23–26]; for example, supersolids [21, 27–30] or quantum magnets [22, 31–33] in optical lattices may exist in the presence of (spin dependent) nearest neighbor interactions. Several techniques have been proposed to create such interactions: exchange interactions in lattices; electric and dipolar interactions; and the interactions between Rydberg atoms. The native exchange interaction in optical lattices [31, 32] is relevant only at the lowest temperatures. In contrast, dipole–dipole interactions can lead to strong long-range interactions, for example, with the native magnetic dipole interaction between atoms with large angular momentum [34, 35], induced electric dipoles in Rydberg atoms or polar molecules. Heteronuclear molecules such as ^{6}Li ^{133}Cs and ^{6}Li ^{87}Rb are particularly interesting due to their large 5.48 and 4.1 D (1 D $\simeq 3.3 \times 10^{-30}$ C-m) electric dipole moments [36]. With those polar molecules, nearest neighbor interactions would be few hundred times stronger than typical for on-site interactions in ultra-cold atomic systems [37]. On the other hand, paramagnetic atoms, e.g., ^{52}Cr with its 6 μ_B magnetic moment generates a magnetic dipole moment induced long-range interaction, which for typical densities is about six times weaker than their s-wave contact interactions [38]. Finally, Rydberg atoms have strong interaction over a very long-range due to their large electric dipole moments [39]. Each of these approaches for creating long-range interactions is possible in principle but is technically challenging.

In this article, we describe coupling between bosons mediated by the exchange of a fermion-hole pair as depicted in Fig. 1. In Sect. 2, we derive an analytic form of this interaction at 2nd order, both directly in perturbation theory and also using the random phase approximation (RPA) [40]. In Sect. 3, we show that 3-body loss process is suppressed as the bosons enter at the Mott-like normal phase. In Sect. 4, we estimate the interaction strength and the loss taking alkaline bosonic and fermionic mixtures as examples. Finally in Sect. 5, we demonstrate that our system leads to a flexible implementation of long-range interactions capable of creating both supersolids or the transverse Ising model in the bosonic system.

2 Theory

Here, we consider a system of two bosons interacting in the presence of a large non-interacting spin-polarized $T = 0$ Fermi gas with N_F particles and density n_F, as shown in Fig. 1a. For simplicity, we assume the fermion density is uniform in the vicinity of bosons. $|\Psi_B(\mathbf{k}_1, \mathbf{k}_2)\rangle$ is the wave function of bosons with momenta $\mathbf{k}_1$ and $\mathbf{k}_2$, and $|\Psi_{\mathrm{DFG}}\rangle$ is the wave function of the ground state of degenerate Fermi

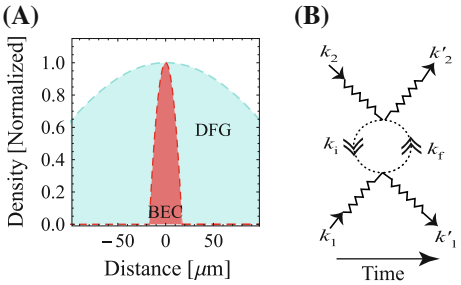

Fig. 1 Essential mechanism for effective Fermi-mediated Bose–Bose interaction. **a** Density distributions of bosons (*red*) and fermions (*blue*) in a harmonic trap of trapping frequency 100 Hz where bosons are embedded in spin-polarized Fermi gas. **b** Schematic of the propagation of fermion-mediated interactions between two long distant bosons. Bosons and fermions are represented by *solid and dashed lines*, respectively

gas (DFG). For uniform systems, the unperturbed ground state energy of the of the gas mixture is

$$E_g = \frac{\hbar^2(k_1^2 + k_2^2)}{2m_B} + \frac{3}{5}N_F\varepsilon_F, \tag{1}$$

where $|g\rangle = |\Psi_B(\mathbf{k}_1, \mathbf{k}_2)\rangle \bigotimes |\Psi_{\mathrm{DFG}}\rangle$. The Fermi energy $\varepsilon_F = \hbar^2 k_F^2/2m_F$ for fermions of mass m_F, Fermi wave vector k_F and Plank's constant $\hbar$. The first-order corrections to E_g arise from interactions between particles. While the bosons can interact with themselves, Pauli blocking does not allow s-wave interaction among spin-polarized fermions, however, that does not prevent s-wave interactions between bosons and fermions. Thus, a boson and a fermion with initial momenta $\mathbf{k}_1$ and $\mathbf{k}_i$ could scatter off each other into final momenta $\mathbf{k}_1'$ and $\mathbf{k}_f$. Over the course of time, the initially scattered fermion-hole pair (with fermion momentum $\mathbf{k}_f$) can interact with the second boson with momentum $\mathbf{k}_2$ and scatter it into $\mathbf{k}_2'$. The fermion simultaneously recombines with the hole, returning to its initial momentum $\mathbf{k}_i$, leaving the Fermi sea unchanged, as depicted in Fig. 1b. This process gives rise to an effective potential between bosons. Any higher-order interactions might lead to a quantitative correction of the Fermi-induced Bose–Bose interactions which is beyond the scope of this article. The Hamiltonians describing the intra- and inter-species interactions can be written in second-quantized notation as

$$\begin{aligned} \hat{H}_{\mathrm{BB}} &= \frac{g_{\mathrm{BB}}}{2}\int d^3\mathbf{r}\hat{\psi}^\dagger(\mathbf{r})\hat{\psi}^\dagger(\mathbf{r})\hat{\psi}(\mathbf{r})\hat{\psi}(\mathbf{r}) \\ \hat{H}_{\mathrm{BF}} &= g_{\mathrm{BF}}\int d^3\mathbf{r}\hat{\psi}^\dagger(\mathbf{r})\hat{\varphi}^\dagger(\mathbf{r})\hat{\psi}(\mathbf{r})\hat{\varphi}(\mathbf{r}), \end{aligned} \tag{2}$$

where $\hat{\psi}(\mathbf{r})$ and $\hat{\varphi}(\mathbf{r})$ are field operators describing the annihilation of bosons and fermions, respectively. $g_{\mathrm{BB}} = 4\pi\hbar^2 a_{\mathrm{BB}}/m_B, g_{\mathrm{BF}} = 2\pi\hbar^2 a_{\mathrm{BF}}(1/m_B + 1/m_F)$ are the intra- and inter-species coupling constants [41, 42]. a_{BF} and a_{BB}

are Bose–Fermi and Bose–Bose s-wave scattering lengths and m_B and m_F are their masses.

2.1 Perturbation method

Due to the exchange of a fermion-hole pair (a second order process), two bosons separated by a distance R will interact [43]. The effective Hamiltonian [44] for the bosonic system describing this fermion-mediated interaction is

$$\begin{aligned}\hat{H}' &= \hat{P}_g \hat{H}_{\rm BF} \sum_{|e\rangle} \frac{|e\rangle\langle e|}{(E_e - E_g)} \hat{H}_{\rm BF} \hat{P}_g \\ &= \sum_{\{\mathbf{k}_1,\mathbf{k}_2\}} |g\rangle \left[\sum_{|e\rangle} \frac{\langle g|\hat{H}_{\rm BF}|e\rangle\langle e|\hat{H}_{\rm BF}|g\rangle}{(E_e - E_g)} \right] \langle g|,\end{aligned} \tag{3}$$

where the projection operator, $\hat{P}_g = \sum_{\{\mathbf{k}_1,\mathbf{k}_2\}} |g\rangle\langle g|$, consists of the sum over all states where the Fermi gas is in its ground state $|\Psi_{\rm DFG}\rangle$. The sum in Eq. (3) includes all states $|e\rangle$ of the joint Bose–Fermi system where the fermionic system is not described by $|\Psi_{\rm DFG}\rangle$. The denominator in Eq. (3) is the unperturbed energy difference of the Bose–Fermi system between states $|g\rangle$ and $|e\rangle$. Using the Fourier transform form of H_BF as given in Eq. (2), the required matrix element (considering the projection in the fermionic sector) in Eq. (3) is

$$\begin{aligned}\langle e|\hat{H}_{\rm BF}|g\rangle = g_{\rm BF} \int \frac{d^3\{\mathbf{k}_1,\mathbf{k}_1',\mathbf{k}_i,\mathbf{k}_f\}}{(2\pi)^9} \hat{\psi}^\dagger(\mathbf{k}_1')\hat{\psi}(\mathbf{k}_1) \\ \times \delta^{(3)}(\mathbf{k}_1 - \mathbf{k}_1' + \mathbf{k}_i - \mathbf{k}_f) \langle e|\hat{\varphi}^\dagger(\mathbf{k}_f)\hat{\varphi}(\mathbf{k}_i)|g\rangle,\end{aligned} \tag{4}$$

where $\delta^{(3)}(\mathbf{k})$ is the Dirac delta function arising from conservation of momentum. Throughout this manuscript, the integration variables are contained between { }-brackets. The combined fermionic part from both of the matrix elements is further reduced to

$$\begin{aligned}&\langle e|\hat{\varphi}^\dagger(\mathbf{k}_f)\hat{\varphi}(\mathbf{k}_i)|g\rangle\langle g|\hat{\varphi}^\dagger(\mathbf{k}_i)\hat{\varphi}(\mathbf{k}_f)|e\rangle \\ &= \Theta(|\mathbf{k}_F - \mathbf{k}_i|)\Theta(|\mathbf{k}_f - \mathbf{k}_F|),\end{aligned} \tag{5}$$

where $\Theta(k)$ represents Heaviside step function. The Θ-function arises from $\langle e|\hat{\varphi}^\dagger(\mathbf{k}_f)\hat{\varphi}(\mathbf{k}_i)|g\rangle$ assuming that $|g\rangle$ describes a $T = 0$ non-interacting Fermi gas. This results from the fact that the first scattering event transfers the fermion from below the Fermi sea to the above and is transferred back in the second scattering.

In this manuscript, we focus on a system of light fermions where $m_F \ll m_B$. In particular, a momentum change $q = |\mathbf{k}_i - \mathbf{k}_f| = |\mathbf{k}_1' - \mathbf{k}_1|$ would have a larger energy cost, $\triangle\epsilon_F$, in light fermions compared to $\triangle\epsilon_B$ in heavy bosons. For a relatively small momentum exchange, $q \le 2k_F$, the ratio of the energy shifts is $\triangle\epsilon_F/\triangle\epsilon_B = (2k_F/q)m^B/m^F \gg 1$. With this assumption, the denominator of Eq. (3) reduces to $\hbar^2(k_f^2 - k_i^2)/2m_F$. With these, Eq. (3) becomes

$$\begin{aligned}\hat{H}' = \frac{1}{2}\int \frac{d^3\{\mathbf{k}_1,\mathbf{k}_1',\mathbf{k}_2,\mathbf{k}_2'\}}{(2\pi)^{12}} \hat{\psi}^\dagger(\mathbf{k}_1')\hat{\psi}(\mathbf{k}_1)\hat{\psi}^\dagger(\mathbf{k}_2')\hat{\psi}(\mathbf{k}_2) \\ \delta^{(3)}(\mathbf{k}_1 - \mathbf{k}_1' + \mathbf{k}_2' - \mathbf{k}_2)\left[G \times \mathcal{F}(|\mathbf{k}_1' - \mathbf{k}_1|)\right],\end{aligned} \tag{6}$$

where $\mathcal{F}(q)$ is the integrated fermionic part described below, which depends on momentum exchange. The associated pre-factor $G = 4m_F g_{\rm BF}^2/\hbar^2$ has dimensions of Energy · Length^4.

Using both Θ-functions and the δ-function, the fermionic contribution simplifies to

$$\mathcal{F}(q) = \frac{(2\pi)^4}{q}\int dk_i \int d(\cos\,\theta)\frac{k_i^2}{q + 2k_i\cos\theta}, \tag{7}$$

where θ is the angle between $\mathbf{k}_i$ and $\mathbf{q}$. The limits of the θ-integration depend on q: For $q \le k_F$, backscattering of fermions at k_F is impossible and k_i will have a lower bound of $(k_F - q)$; in an intermediate range, $k_F \le q \le 2k_F$, fermions up to $(q - k_F)$ can be backscattered and the rest will be restricted to scatter within a range of angle θ_ℓ described below and lastly when $q \ge k_F$ the integration is unrestricted. The Heaviside step function $\Theta(|\mathbf{k}_f - \mathbf{k}_F|) \equiv \Theta(|\mathbf{q} + \mathbf{k}_i - \mathbf{k}_F|)$ implies the maximum scattering angle $\cos\theta_\ell = (k_F^2 - k_i^2 - q^2)/2qk_i$. For any q, Eq. (7) integrates to

$$\mathcal{F}(q) = \frac{(2\pi)^4}{16q}\left[2k_F q + (4k_F^2 - q^2)\tan\,h^{-1}\left|\frac{2k_F}{q}\right|\right]. \tag{8}$$

Since the magnitude of $\mathcal{F}(q)$ drops monotonically with q as shown in Fig. 2, the effective Bose–Bose interactions favor small momentum exchange.

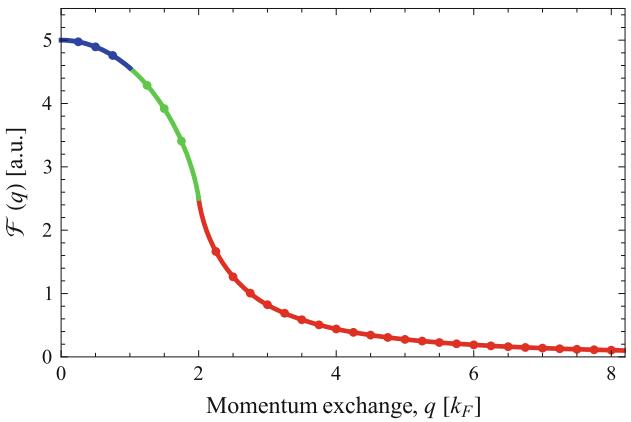

Fig. 2 Distribution of $\mathcal{F}(q)$ as a function of momentum exchange q at three different domains i.e., $|\mathbf{q}| \le |\mathbf{k}_F|$ (*blue*), $|\mathbf{k}_F| \le |\mathbf{q}| \le 2|\mathbf{k}_F|$ (*green*), $|\mathbf{q}| \ge 2|\mathbf{k}_F|$ (*red*)

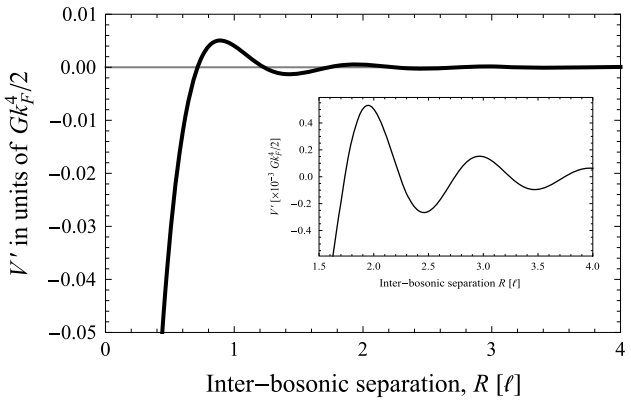

Fig. 3 The spatial dependence of the fermion-mediated Bose–Bose interaction V' is shown in an arbitrary unit (a.u.)

The spatial dependence of H' can be obtained from the Fourier transform of Eq. (6). The inverse Fourier transformation of the bosonic field operators reduces Eq. (6) to

$$H' = \frac{1}{(2\pi)^5}\int \frac{d^3\{\mathbf{r}_1,\mathbf{r}_2\}}{|\mathbf{r}_1-\mathbf{r}_2|}\Big[\hat{\psi}^\dagger(\mathbf{r}_1)\hat{\psi}(\mathbf{r}_1)\hat{\psi}^\dagger(\mathbf{r}_2)\hat{\psi}(\mathbf{r}_2) \; G\int_0^\infty \mathrm{d}q\, q\mathcal{F}(q)\sin q|\mathbf{r}_1-\mathbf{r}_2|\Big], \tag{9}$$

where $|\mathbf{r}_1 - \mathbf{r}_2| = R$ denotes the separation between bosons. The remaining integral over q can be evaluated [45], giving

$$H' = \frac{1}{2}\int d^3\{\mathbf{r}_1,\mathbf{r}_2\}\hat{\psi}^\dagger(\mathbf{r}_1)\hat{\psi}^\dagger(\mathbf{r}_2)V'(r_1-r_2)\hat{\psi}(\mathbf{r}_2)\hat{\psi}(\mathbf{r}_1), \tag{10}$$

with an effective potential

$$V'(R) = -\frac{Gk_F^4}{2}\frac{\sin 2k_FR - 2k_FR\cdot\cos 2k_FR}{(2k_FR)^4}. \tag{11}$$

This potential, an ultra-cold atom analog of the RKKY potential, has nonzero range, and is modulated on a characteristic length scale $\ell = \pi/k_F$.

The spatial dependence of $V'(R)$ is shown in Fig. 3. The inter-boson separation R is given in units of ℓ derived from the Fermi wave vector. The amplitude of the Friedel-type oscillations decays at longer separation of bosons [46, 47]. The effective potential $V'(R)$ is identical to the RKKY interaction in solids, where two nuclear spins interact by exchanging a conduction electron-hole pair [48–50]. RKKY interactions are important in many systems, for example, in ferromagnetic layers isolated by non-magnetic metal layer [51, 52] and possibly in iron-based superconductors [53].

2.2 Random phase approximation

A second approach to this problem is to identify a response or screening function in the system. In our case, each boson locally alters the fermion density leading to a long-range density modulations described by response function χ [21]. Linear response theory can be used, provided the fermion density is only slightly changed. This approximation method leads the fermion-mediated boson–boson interaction energy to

$$H' = \int d^3\mathbf{r}\, g_{\mathrm{BF}}^2\chi(r_1-r_2)\hat{\psi}^\dagger(\mathbf{r}_1)\hat{\psi}(\mathbf{r}_1)\hat{\psi}^\dagger(\mathbf{r}_2)\hat{\psi}(\mathbf{r}_2), \tag{12}$$

where $\chi(r_1 - r_2)$ is the Lindhard response function [54]. In this expression, we used the static response function, which implies that the light fermions redistribute their density on time scale rapid compared to the dynamical time scale of the bosonic subsystem. Now considering the momentum of the fermion below Fermi level is $\mathbf{k}_i = \mathbf{k} - \mathbf{q}/2$ and above $\mathbf{k}_f = \mathbf{k} + \mathbf{q}/2$ (Fig. 1), the response function in terms of fermion's momentum is

$$\chi(q) = \int \frac{d^3\mathbf{k}}{(2\pi)^3}\frac{f[\epsilon(\mathbf{k}-\mathbf{q}/2)] - f[\epsilon(\mathbf{k}+\mathbf{q}/2)]}{\epsilon(\mathbf{k}-\mathbf{q}/2) - \epsilon(\mathbf{k}+\mathbf{q}/2) + i\eta}, \tag{13}$$

where $f(\epsilon)$ is the probability distribution function of Fermions at any energy, ϵ, and η is the retardation parameter. For non-interacting Fermi gas the distribution function is

$$f(\epsilon) = \Theta(\epsilon_F - \epsilon). \tag{14}$$

This implies $f(\epsilon(\mathbf{k}-\mathbf{q}/2)) - f(\epsilon(\mathbf{k}+\mathbf{q}/2)) = \Theta(\epsilon(\mathbf{k}_F) - \epsilon(\mathbf{k}))$, so Eq. (13) reduces to

$$\chi(q) = -\frac{2m_F}{(2\pi\hbar)^2}\left(\frac{1}{q}\int_0^{k_F}\mathrm{d}k\, k\log\left|\frac{2k-q}{2k+q}\right|\right). \tag{15}$$

The integrand in the above equation is identical to that in Eq. (7) following integration over θ, showing that both approaches give the same result.

2.3 Discussion

This fermion-mediated effective boson–boson interaction can be compared with the bare bosonic interaction. Consider a sufficiently dilute Bose gas, where $V'(R)$ can itself be replaced with a contact potential. The corresponding contact interaction potential is of the form of $V(r_1 - r_2) = g'\cdot\delta(r_1 - r_2)$. In the Born approximation, i.e., $q \to 0$, the effective boson–boson coupling constant is $g' = \int d^3R V'(R)$, which becomes

$$g' = -\frac{4\pi\hbar^2}{m_B}\left[\frac{1}{32k_F}\cdot\frac{m_B}{m_F}\left(\frac{g_{\mathrm{BF}}k_F^3}{\epsilon_F}\right)^2\right]. \tag{16}$$

Here, the effective scattering length, defined by

$$a_{eff} = \frac{9\pi^4 m_B}{8k_F m_F}\left(\frac{g_{\rm BF} n_F}{\epsilon_F}\right)^2, \tag{17}$$

is tuned either by Feshbach resonance or by changing the fermion density, since $k_F = (6\pi^2 n_F)^{1/3}$. Because $g' \propto g_{\rm BF}^2$, the effective contact interaction is always attractive. This need not be the case for interactions between bosons in different hyperfine states. We use notations, $\uparrow$ and $\downarrow$, to represent bosons in two different spin states. The new coupling constant, $g'_{\uparrow\downarrow} \propto g_{\uparrow F} \cdot g_{\downarrow F}$, can be either attractive or repulsive depending on the signs of $g_{\uparrow F}$ and $g_{\downarrow F}$. Additionally $g'_{\uparrow\downarrow}$ can be tuned using a Feshbach resonance that changes just one of $g_{\uparrow F}$ or $g_{\downarrow F}$. As an example, coupling constants $g', g'_{\uparrow\downarrow}$ and $g_{\rm BB}$ are compared in Sect. 4 for Bose–Fermi mixtures of $|^{87}\mathrm{Rb}; 1, 1\rangle = \uparrow, |^{87}\mathrm{Rb}; 1, 0\rangle = \downarrow$ and ^{6}Li.

Given that the effective potential can be comparable in strength to the boson contact interaction, we now focus on the important fact that $V'(R)$ has a non-negligible range $\propto \pi/k_F$ (see inset to Fig. 3). The spatial dependence at any short range is quite unlike to the dipole–dipole interaction potential which varies $V_{\rm dipole}(R) \propto 1/R^3$, instead the short-range interaction $V'(R) \propto 1/R$. Remarkable work on creating ultra-cold molecules [55] and Rydberg atoms [56] with large electric dipole moments or producing condensates of atoms with large magnetic moments [57] ia a step forward to study many-body dynamics associated with long-range forces. In comparison to the dipole-dipole interaction, the new V' is isotropic in space. (Although a spatial dependence of fermion density $n_F(R)$ will lead to anisotropic position-dependent interaction.) In addition, both the magnitude and sign of V' is tunable with the help of Feshbach resonances, a freedom that is unavailable for dipole–dipole interactions. Thus, these mediated interactions can access a different class of many-body systems than dipolar gases can.

3 Suppression of three body recombination

Three-body ($3N$) recombination—a common loss mechanism in ultra-cold atom systems—is a process where three incoming atoms collide, and two form a bound state; this dimer and the remaining atom carry out the binding energy, simultaneously conserving momentum. The $3N$-loss rate is $\mathrm{d}n/\mathrm{d}t \propto n^3$, and this loss generally dominates for atomic densities $n \gtrsim 10^{15}\,\mathrm{cm}^{-3}$ [58]. Near Feshbach resonances, the scattering length a changes rapidly and the rate constant is enhanced. For recombination of three identical bosons, the $3N$-loss rate is proportional to a^4 [59, 60]; in contrast, for two bosons and a third atom of different species that rate is instead proportional to a^2 [61] for a Bose–Bose scattering length a.

In mixtures of s-wave interacting bosons and spin-polarized fermions, the formation of Fermi–Fermi bound states is greatly suppressed. Thus, in such mixtures, $3N$-recombination is dominated by the formation of Bose–Bose dimers, B_2 and Bose–Fermi dimers BF. Generally, sufficiently near inter-species Feshbach resonances, the $3N$-recombination is dominated by the formation of BF-dimers; this process can become the limiting factor in experiment by reducing the lifetime of the atomic ensemble by orders of magnitude [70]. We propose to use bosons in a Mott-like normal state with single occupation per lattice site while the fermions still form a free Fermi gas, absent of any significant lattice potential. This combination can greatly reduce the $3N$-recombination rate. The rate equation for the average loss of bosons $\langle N\rangle$ from lattice is modified to

$$\frac{\mathrm{d}}{\mathrm{d}t}\langle N\rangle = -K_3 \int d^3 r \langle n^3\rangle, \tag{18}$$

where K_3 is the rate coefficient for $3N$-recombination. In our gas mixtures, the quantity $\langle n^3\rangle$ is derived from $\langle \hat{n}_B(\hat{n}_B - 1)(\hat{n}_B - 2)\rangle$ and $\langle \hat{n}_B(\hat{n}_B - 1)\rangle\langle n_F\rangle$ for the $3N$-formation of dimer-atom pairs $B_2 + B$, $B_2 + F$ and $\mathrm{BF} + B$, respectively. The $\mathrm{BF} + B$ channel generally dominates near inter-species Feshbach resonances. Here, we assume that fermions are distributed over a larger spatial region than the lattice bosons (Fig. 1a); hence, n_F is taken to be homogeneous. In this section, we estimate $3N$-recombination rate of bosons confined in a three-dimensional optical lattice, by obtaining $\langle n^d\rangle = \langle \prod_{n'=0}^{d-1}(n_B - n')\rangle$ (integer d) from the finite temperature Bose–Hubbard model.

The Bose–Hubbard Hamiltonian, including fermion-mediated nearest neighbor interactions, is extended to

$$\hat{H}_{BH} = -t\sum_j (\hat{b}_j^\dagger \hat{b}_{j+1} + h.c.) + \frac{U}{2}\sum_j \hat{n}_{B,j}(\hat{n}_{B,j} - 1) - \mu\sum_j \hat{n}_{B,j} + V\sum_j \hat{n}_{B,j}\hat{n}_{B,j+1}, \tag{19}$$

where $\hat{b}_j^\dagger$ ($\hat{b}_j$) are the creation (annihilation) operators at the j-th lattice site; $\hat{n}_{B,j} = \hat{b}_j^\dagger \hat{b}_j$ is the boson density; t is the amplitude for hopping from one site to the next; U and V represent the on-site and fermion-mediated nearest neighbor interactions between bosons; and μ is the bosonic chemical potential. The first order effect of the fermions, as given in Eq. (10), is to shift the chemical potential to $\mu = \tilde{\mu} + g_{\rm BF} \cdot \langle n_F\rangle$, where $\langle n_F\rangle$ is the local fermion density. Fermion-mediated interactions beyond the nearest neighbor are in principle present (Fig. 6b), and important depending on $\langle n_F\rangle$, however, we choose to focus on a Fermi system

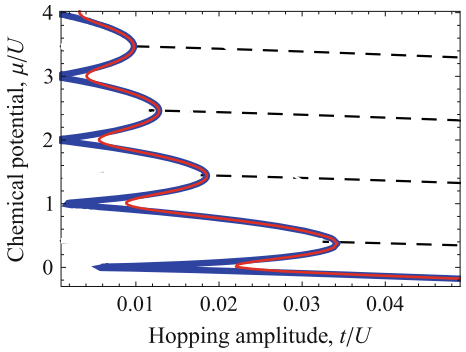

Fig. 4 Mean field phase diagram of the 3D Bose–Hubbard model showing Mott-like normal to superfluid transition at temperatures $k_B T = 0$, and $0.05U$. The *blue curve* indicates the zero temperature phase diagram and the *red curve* is for nonzero temperature. The *black dashed lines* denote the contours of integer boson density at $T = 0$

for which the nearest neighbor interaction dominates. The effective V can be obtained by expressing the continuum bosonic field operators in terms of Wannier functions $\omega(r)$ as $\hat{\psi}_j = \hat{b}_j \omega(r)$ [similarly $\hat{\psi}_j^\dagger = \hat{b}_j^\dagger \omega^*(r)$].

To estimate the rate of $3N$-recombination, we performed a mean field calculation of the Bose–Hubbard Hamiltonian using the decoupling approximation [62, 63]. In this approximation, we can compute the desired local correlation functions as well as the superfluid order parameter $\langle \hat{b}_i \rangle$. The phase diagrams for equilibrium bosons at $k_B T = 0$ and $0.05U$ are shown in Fig. 4. With this knowledge of Mott-like normal (normal) and superfluid (SF) phases at any values of t and U, we compute the expectation values relevant to the $3N$-recombination in individual lattice sites

$$\left\langle \prod_{n'=0}^{d-1} (n_B - n') \right\rangle = \int_0^\infty d^3 r |\omega(r)|^2 \prod_{n'=0}^{d-1} (n_{B,j} - n'), \qquad (20)$$

where $d = 2$ and 3 for their integer numbers. In the following section we compute the $3N$-loss rate in the ^{87}Rb–^{6}Li system.

4 Alkali Bose–Fermi mixtures

Alkali-metal atoms are widely used in ultra-cold atom experiments due to their well-understood properties and relatively straightforward laboratory implementation. Among them, the non-radioactive bosonic species are ^{7}Li, ^{23}Na, ^{39}K, ^{41}K, ^{85}Rb, ^{87}Rb, ^{133}Cs, and the fermionic species are ^{6}Li, ^{40}K. Figure 5 shows the strength of fermion-mediated effective Bose–Bose scattering g', as given in Eq. (16), is estimated for various possible alkaline Bose–Fermi gas mixtures. In this section, we identify the optimal alkali Bose–Fermi mixtures (^{87}Rb–^{6}Li or ^{133}Cs–^{6}Li, although the scattering properties of the later are unknown), where bosons are deeply bound in an optical lattice in the presence of nominally free fermions. Further, we investigate the loss rate of atoms due to $3N$-recombination and compare different interactions present in a Bose–Fermi mixture as described in Sect 2.

The periodicity of a three-dimensional optical lattice potential, $V(r) = V_0 \sum_{u=x,y,z} \sin^2(k_r u)$, depends on the $k_r = 2\pi/\lambda$ wave vector of the lattice laser, i.e., at a wavelength λ. The depth of the potential $V_0 = -I\alpha(\lambda)/2\varepsilon_0 c$ is a function of wavelength-dependent polarizability $\alpha(\lambda)$, and optical intensity I. Here ε_0 is free space permittivity, c is velocity if light. We use $\lambda = 1{,}064$ nm throughout this article. Values of $\alpha(\lambda)$ and the photon recoil energy $E_r(\lambda) = h^2/2m\lambda^2$ for the alkaline elements are listed in Table 1.

The lattice depth for the alkali atoms are also compared in Fig. 6a. Physically one can also understand Fig. 6 that a heavy boson would be more localized in an optical lattice due to its small E_r where as light fermions would hardly experience the lattice.

^{87}Rb and ^{6}Li have a mass ratio $m_B/m_F = 14.5$: an excellent combination for investigating the interaction described in this article (Fig. 6). The coupling constants g' and $g'_{\uparrow\downarrow}$ for a binary $|^{6}\mathrm{Li}; 1/2, 1/2\rangle \otimes |^{87}\mathrm{Rb}; 1, 1\rangle$ system and for mixtures of $|^{6}\mathrm{Li}; 1/2, 1/2\rangle \otimes (|^{87}\mathrm{Rb}; 1, 1\rangle + |^{87}\mathrm{Rb}; 1, 0\rangle)$ are shown in Fig. 7 near the vicinity of the $|^{6}\mathrm{Li}; 1/2, 1/2\rangle \otimes |^{87}\mathrm{Rb}; 1, 1\rangle$ Feshbach resonance. The resonance has been experimentally located at magnetic field $B_0 = 106.692$ mT and has a width $\delta B = 1.062$ mT [70]. The coupling constant g' is magnetically tunable and scales like $(1 + \delta B/|B - B_0|)^2$. Using the effective

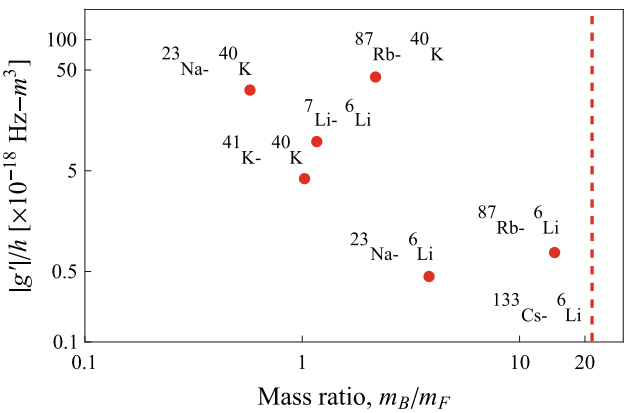

Fig. 5 Variation of effective boson–boson coupling constant g'/h at $k_F = 2\pi/\lambda$ with boson to fermion mass ratio m_B/m_F for possible Bose–Fermi mixtures of non-radioactive alkali atoms. The inter-species scattering lengths are adopted from following references ^{23}Na–^{40}K [64], ^{7}Li–^{6}Li [65], ^{41}K–^{40}K [66], ^{87}Rb–^{40}K [67], ^{23}Na–^{6}Li [68], ^{87}Rb–^{6}Li [18]. The ^{133}Cs–^{6}Li scattering length is currently unknown, we therefore do not specify g'

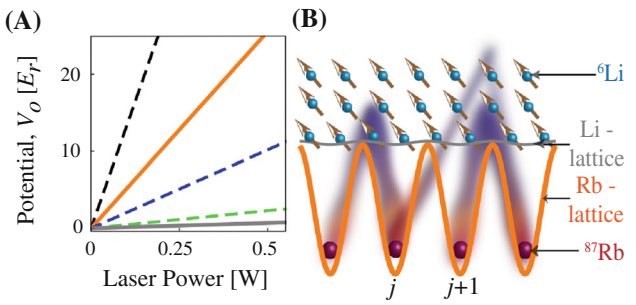

Fig. 6 **a** Depth of the lattice potential of alkali atoms: Li (*gray*), Na (*green*), K (*blue*), Rb (*orange*) and Cs (*black*) in an optical lattice constructed of laser at wavelength $\lambda = 1{,}064$ nm. **b** Artistic view of long-range interactions among deeply bound ^{87}Rb atoms in the optical lattice, which are mediated by nearly free spin-polarized ^{6}Li in the same environment. The estimated next nearest neighbor interaction for Fermi density 2×10^{13}cm $^{-3}$ and lattice spacing 532 nm is three orders of magnitude weaker than the nearest neighbor interaction

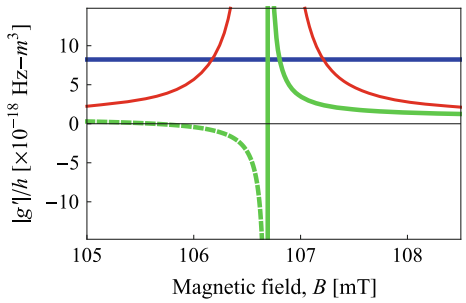

Fig. 7 Dependence of g' (red), $g'_{\uparrow\downarrow}$ (*green*) and g_{BB} (*blue*) for $(|^{87}\mathrm{Rb}; 1, 1\rangle + |^{87}\mathrm{Rb}; 1, 0\rangle) \otimes {}^6\mathrm{Li}|1/2, 1/2\rangle$ mixtures on magnetic field. The $|^{87}\mathrm{Rb}; 1, 1\rangle \otimes {}^6\mathrm{Li}|1/2, 1/2\rangle$ Feshbach resonance at the magnetic field of 106.692 mT tunes the $|^{87}\mathrm{Rb}; 1, 1\rangle$ - $|^6$ Li$; 1/2, 1/2\rangle$ interactions. *Dashed and solid lines* distinguish the repulsive and attractive interactions

Table 1 Single photon recoil energy E_r and polarizabilities $\alpha(\lambda)$ at wavelength $\lambda = 1{,}064$ nm for some common alkaline-metal atoms [69]

	^{6}Li	^{23}Na	^{40}K	^{87}Rb	^{133}Cs
E_r [$\times 10^{-30}$ J]	19.3	5.03	2.89	1.33	0.87
α [A^2 s^4 Kg^{-1}]	270.8	233.6	597.5	689.9	1,162.1

interaction g' and $g'_{\uparrow\downarrow}$, the $|^6\mathrm{Li}; 1/2, 1/2\rangle \otimes (|^{87}\mathrm{Rb}; 1, 1\rangle + |^{87}\mathrm{Rb}; 1, 0\rangle)$ mixtures opens the possibility to tune the $g'_{\uparrow\downarrow} \propto 1 + \delta B/(B - B_0)$ on either of the attractive or repulsive sides with the same magnetic field. The Bose–Bose interaction is constant over this magnetic field range (Fig. 7) due to absence of any Feshbach resonances [71]. All different types of interactions become comparable when $B - B_0 = \delta B/2$ a region of particular interest for future investigations (Sect. 5).

In a ^{87}Rb–^{6}Li mixture, Rb_2 dimers can form from collisions between $3 \times$ Rb or $2 \times$ Rb + Li atoms; near the Feshbach resonance, the rate of Rb Li dimer formation is enhanced by four orders of magnitude. The rate coefficients for all $3N$-recombination channels in a ^{87}Rb–^{6}Li mixtures are listed in the Table 2.

The computed $3N$-loss rates for Rb_2 + Rb, Rb_2 + Li and Rb + Rb Li channels at both normal phase with single occupation per site and SF phases are shown in Fig. 8a. In the SF region, Rb_2 + Rb recombination channel is more likely since the intra-species scattering length $a_{\text{Rb-Rb}}$ is five times larger than the inter-species scattering length $a_{\text{Rb-Li}}$. In that region, the collision rate of the non-localized atoms increases; thus, recombination increases monotonically with density and hence μ. In a normal phase with less than three ^{87}Rb atoms per site, formation of Rb_2-dimer by $3 \times$ Rb recombination is prohibited. Also, the $2 \times$ Rb + Li collision is blocked with single-site occupation, of ^{87}Rb. In the higher Mott-lobes with increased ^{87}Rb occupation $\langle n_B \rangle$, the loss rate is quadratic in $\langle n_B \rangle$ for $2 \times$ Rb + Li collision and cubic in $\langle n_B \rangle$ for $3 \times$ Rb collision (Fig. 8b). Thus, a normal phase with $\langle n_B \rangle = 1$ will suppress atoms loss through all $3N$-recombination channels even at the Feshbach resonance. This allows the practical creation of strong fermion-mediated boson–boson interactions comparable in strengths with on-site interaction.

5 Many-body systems

Large fermion-mediated interactions between bosons in neighboring lattice sites and beyond opens the door for studying a range of unexplored many-body phases. In this section, we discuss how SS and quantum magnetic (QM) phases can be realized in the bosonic component of ^{87}Rb–^{6}Li mixtures with bosons localized in the sites of an optical lattice. The fermion-mediated interactions, as given in Eq. (10), gives the extended Bose–Hubbard [Eq. (19)] nearest neighbor (NN) potential

$$V = \int_0^\infty d^3\{\mathbf{r}_1, \mathbf{r}_2\} |w(\mathbf{r}_1 - \mathbf{r}_j)|^2 \\ V'(|\mathbf{r}_{j+1} - \mathbf{r}_j|) |w(\mathbf{r}_2 - \mathbf{r}_{j+1})|^2, \tag{21}$$

where $|\mathbf{r}_{j+1} - \mathbf{r}_j| = \lambda/2$ is the lattice spacing (Fig. 6b), and $w(\mathbf{r}_j)$ is the Wannier function [74] describing a boson localized in the j-th lattice site.

For these nearest neighbor interactions to be relevant at current experimental temperature scales, V should be comparable to the U native on-site contact interactions

Table 2 List of $3N$-recombination processes in the mixture of bosonic ^{87}Rb and fermionic ^{6}Li gases in the lowest energy Zeeman sublevels $|^{87}\text{Rb}; 1, 1\rangle$ and $|^{6}\text{Li}; 1/2, 1/2\rangle$, respectively. For Feshbach-enhanced recombination, the magnetic fields are listed

Recombination type	K_3 [cm^6/s]	Magnetic field [mT]	Scattering channel
$3 \times$ Rb	10^{-28} [72, 73]	(Background)	s-wave
$2 \times$ Rb + Li	$(6.7 - 44) \times 10^{-29}$ [70]	(Background)	s-wave
$2 \times$ Rb + Li	$(1.1 - 6.1) \times 10^{-26}$ [70]	88.202	s-wave
$2 \times$ Rb + Li	$(7.9 - 67) \times 10^{-26}$ [70]	106.692	s-wave
$3 \times$ Li	$(2.4 - 20) \times 10^{-24}$ [70]	15.855	p-wave
Rb + $2 \times$ Li	$(4.7 - 95) \times 10^{-26}$ [70]	15.855	p-wave

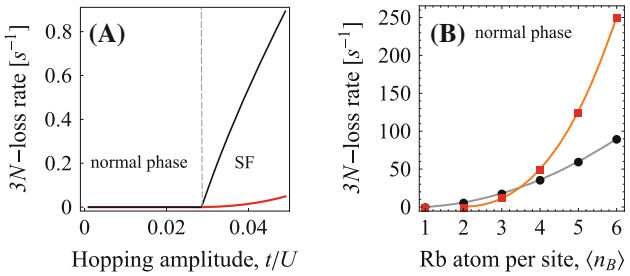

Fig. 8 Three body decay rates far from the Feshbach resonance due to the formation of Rb_2 + Rb (*red*) and Rb_2 + Li (*black*) pairs: **a** for $\langle n_i \rangle = 1$ starting in the normal phase and crossing into the SF region, **b** in the normal phase at $T = 0.05U$ for $\langle n_i \rangle \geq 1$ (commensurate fillings). In this plot, we considered ^{87}Rb atoms in the lowest Bloch band of a $20E_r$ deep optical lattice and with fermion density $n_F = 2 \times 10^{13}$ cm^{-3} (corresponding to a Fermi wave vector $k_F = 2\pi/\lambda$, matched to the $\lambda = 1{,}064$ nm optical wavelength)

$$U = g_{\text{BB}} \int_0^\infty d^3\mathbf{r}_1 |w(\mathbf{r}_1)|^4. \tag{22}$$

For ^{87}Rb, U is repulsive and on the order of kHz for lattice depths in the $5E_r$ to $20E_r$ range and the $V_{\text{ex}} = 2t^2/U$ nearest neighbor exchange energy is at most at the Hz energy scale for a unit filled MI. Figure 9 compares the strength of the nearest neighbor interactions V to the native on-site interactions U.

The thermal energy of a BEC in an optical lattice depends on the lattice depth and is typically cooler than the same BEC before the lattice was applied (due to adiabatic cooling) [75]. Even with this cooling, currently achieved temperatures are still large compared to V_{ex}. Thus, many-body physics due to V_{ex} remains experimentally unrevealed. However, the Feshbach-tunable fermion-mediated nearest neighbor interaction is a much larger artificial magnetic interaction between bosons.

In many theoretical studies [21, 28–30], SS phases have been predicted for the Hamiltonian in Eq. (19). Our model system should realize a SS phase when the mediated NN interaction becomes comparable to the on-site U. A repulsive NN coupling between identical bosons can be obtained when the lattice spacing d is comparable to the

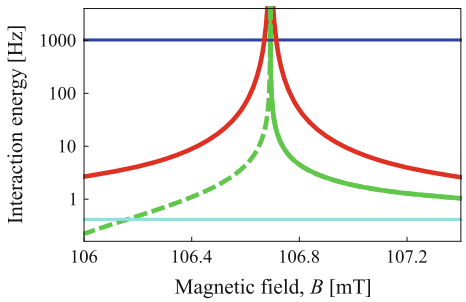

Fig. 9 Tuning of fermion-mediated nearest neighbor interactions with magnetic field for various combinations of ^{87}Rb spin states that are immersed in a ^{6}Li bath. The coupling constants are computed for ^{87}Rb atoms arrayed in a 532 nm period optical lattice: atoms in $|^{87}\text{Rb}; 1, 0\rangle$ interacting with strength $V_{\downarrow\downarrow}$ (*cyan*), $|^{87}\text{Rb}; 1, 1\rangle$ interacting with strength V (*red*), a mixture of both spin states interacting with strength $V_{\uparrow\downarrow}$ (*green*) and the on-site s-wave interaction of ^{87}Rb atoms U (*blue*). Repulsive (attractive) interactions are denoted by *dashed* (*solid*) curves. In this plot, we consider the 106.692 mT $|^{87}\text{Rb}; 1, 1\rangle \otimes |^{6}\text{Li}; 1/2, 1/2\rangle$ Feshbach resonance

first peak of the Friedel oscillation in $V'(r)$, i.e., $d = 0.9\ \ell$ in Fig. 3. A repulsive NN interaction at this lattice spacing can be obtained by proper choice of Fermi density n_F. A typical experiment would start with a unit occupancy MI state ($\langle n_B \rangle = 1$ and $U \gg zV$ for z number of nearest neighbors). Subsequently, tuning the NN interaction such that $(zV - U)/2 \approx t$ would yield a SS phase for average boson densities between 1/2 and 1 per site [76, 77]. This can be achieved by adiabatically relaxing the external trapping potential as t and V are increased. At larger $\langle n_B \rangle$, phase separation is expected.

Quantum magnetism is another very interesting phenomena [22]. Experimentally, such phases have been realized with chain of trapped ions [78] also recently with ultracold atoms in an optical lattice [79, 80]. In our system, QM phases can be created with two different hyperfine states realizing a pseudo-spin 1/2 system, where $|\uparrow\rangle$ and $|\downarrow\rangle$ label the two spin components $|^{87}\text{Rb}; 1, 1\rangle$ and $|^{87}\text{Rb}; 1, 0\rangle$, respectively. The Hamiltonian including the fermion-mediated interactions of these pseudo- spin-1/2 bosons is

$$\begin{aligned}\hat{H}_{BH}^{\uparrow\downarrow} = &-\mu\sum_{\sigma,j}\hat{n}_{\sigma,j}^{B} - t\sum_{\sigma,j}\left[\hat{b}_{\sigma,j}^{\dagger}\hat{b}_{\sigma,j+1} + \text{h.c.}\right] \\ &+ \frac{U}{2}\sum_{\sigma,j}\hat{n}_{\sigma,j}^{B}(\hat{n}_{\sigma,j}^{B} - 1) + U\sum_{j}\hat{n}_{\uparrow,j}^{B}\hat{n}_{\downarrow,j}^{B} \\ &+ V^{\downarrow\downarrow}\sum_{j}\hat{n}_{\downarrow,j}^{B}\hat{n}_{\downarrow,j+1}^{B} + V\sum_{j}\hat{n}_{\uparrow,j}^{B}\hat{n}_{\uparrow,j+1}^{B} \\ &+ \frac{V^{\uparrow\downarrow}}{2}\sum_{j}\hat{n}_{\uparrow,j}^{B}\hat{n}_{\downarrow,j+1}^{B},\end{aligned} \tag{23}$$

where $\hat{b}_{\sigma,j}^{\dagger}$ describes the creation of a boson in site j with spin $\sigma \in \{\uparrow, \downarrow\}$ and the spin-dependent NN interactions are tunable by Feshbach resonance as shown in Fig. 9. In this model, the hoping, on-site interaction, and effective chemical potential are all state independent. The Schwinger boson representation [81], i.e.,

$$\begin{aligned}\hat{S}_{j}^{x} &= \frac{1}{2}\left(\hat{b}_{\uparrow,j}^{\dagger}\hat{b}_{\downarrow,j} + \hat{b}_{\downarrow,j}^{\dagger}\hat{b}_{\uparrow,j}\right) \\ \hat{S}_{j}^{y} &= -\frac{1}{2}\mathrm{i}\left(\hat{b}_{\uparrow,j}^{\dagger}\hat{b}_{\downarrow,j} - \hat{b}_{\downarrow,j}^{\dagger}\hat{b}_{\uparrow,j}\right) \\ \hat{S}_{j}^{z} &= \frac{1}{2}\left(\hat{b}_{\uparrow,j}^{\dagger}\hat{b}_{\uparrow,j} - \hat{b}_{\downarrow,j}^{\dagger}\hat{b}_{\downarrow,j}\right) = \frac{1}{2}\left(\hat{n}_{\uparrow,j}^{B} - \hat{n}_{\downarrow,j}^{B}\right) \\ \hat{n}_{j}^{B} &= \hat{n}_{\uparrow,j}^{B} + \hat{n}_{\downarrow,j}^{B},\end{aligned} \tag{24}$$

represents the Hamiltonian [Eq. (23)] in terms of spin operators. A spin model for ultra-cold atoms in an optical lattice with only exchange induced NN interactions was studied by Duan et al. [31], and we add the effect of tunable true NN interactions. Neglecting the effect of the tunneling and on-site interactions, the spin model from the remainder of Eq. (23) is

$$\begin{aligned}\hat{H}_{S} = &\alpha(B)\sum_{j}\hat{n}_{j}^{B}\hat{n}_{j+1}^{B} + 2\beta(B)\sum_{j}\hat{n}_{j}^{B}\cdot\hat{S}_{j+1}^{z} \\ &+ \gamma(B)\sum_{j}\hat{S}_{j}^{z}\cdot\hat{S}_{j+1}^{z},\end{aligned} \tag{25}$$

where $\alpha(B) = (V + V^{\downarrow\downarrow} + 2V^{\uparrow\downarrow})$, $\beta(B) = (V - V^{\downarrow\downarrow})$ and $\gamma(B) = V + V^{\downarrow\downarrow} - 2V^{\uparrow\downarrow}$ are Feshbach tunable. The first term in $\hat{H}_S$ gives only a net shift of the mean energy, the second term gives interaction of atoms with the magnetic field produced by next lattice sites and the last term gives interaction between transverse components of the magnetic fields produced at the consecutive sites. Together, these form a quantum Ising pseudo-spin model with longer-range spin correlation in neutral atoms. Although the spontaneous magnetic ordering takes place at a temperature typically three orders of magnitude smaller than the achievable temperature in current experiments, the Feshbach-enhanced NN pseudo-spin interaction can overcome the thermal energy and various intriguing many-body phases might be enlightened.

6 Conclusions

In this Article, we described a way of creating long-range interactions between distant bosons mediated by the exchange of fermions excited from a spin-polarized, non-interacting, degenerate Fermi gas. A mixture of heavy bosons and light fermions is ideal because a lattice will localize bosons while the fermions can move freely. The $3N$-recombination will greatly be suppressed in the unit occupied bosonic Mott-like normal phase. This proposal takes advantage of the Feshbach tunability of the NN interaction that might create SS and QM phases in ultra-cold bosons.

Acknowledgments We had very useful discussions with A. Gangopadhyay, R. Sensarma, A. Sen Gupta and W. D. Phillips. This work was carried out as a part of STIOS program funded by CSIR-NPL. We also acknowledge the financial support the NSF through the Physics Frontier Center at JQI, and the ARO with funds from both the Atomtronics MURI and the DARPA OLE Program.

References

1. L.N. Cooper, Phys. Rev. **104**, 1189 (1956)
2. H. Heiselberg, C.J. Pethick, H. Smith , L. Viverit, Phys. Rev. Lett. **85**, 2418 (2000)
3. M.J. Bijlsma, B.A. Heringa, H.T.C. Stoof, Phys. Rev. A **61**, 053601 (2000)
4. L. Viverit, Phys. Rev. A **66**, 023605 (2002)
5. F. Matera, Phys. Rev. A **68**, 043624 (2003)
6. J. Bardeen, G. Baym, D. Pines, Phys. Rev. Lett. **17**, 372 (1966)
7. D.V. Efremov, L. Viverit, Phys. Rev. B **65**, 134519 (2002)
8. K. Suzuki, T. Miyakawa, T. Suzuki, Phys. Rev. A **77**, 043629 (2008)
9. M. Lewenstein, L. Santos, M.A. Baranov, H. Fehrmann, Phys. Rev. Lett. **92**, 050401 (2004)
10. M. Rinck, C. Brude, Phys. Rev. A **83**, 023608 (2011)
11. A. Schirotzek, C.H. Wu, A. Sommer, M.W. Zwierlein, Phys. Rev. Lett. **102**, 230402 (2009)
12. P.A. Lee, N. Nagaosa, X.-G. Wen, Rev. Mod. Phys. **78**, 17 (2006)
13. G. Modugno, G. Roati, F. Riboli, F. Ferlaino, R.J. Brecha, M. Inguscio, Science **27**, 2240 (2002)
14. S. Nascimbène, N. Navon, K.J. Jiang, F. Chevy, C. Salomon, Nature **463**, 1057 (2010)
15. G. Modugno, G.Ferrari, G. Roati, R.J. Brecha, A. Simoni, M. Inguscio, Science **292**, 2570 (2001)
16. G. Roati, F. Riboli, G. Modugno, M. Inguscio, Phys. Rev. Lett. **89**, 150403 (2002)
17. Z. Hadzibabic, C.A. Stan, K. Dieckmann, S. Gupta, M.W. Zwierlein, A. Görlitz, W. Ketterle, Phys. Rev. Lett. **88**, 160401 (2002)
18. C. Silber, S. Günther, C. Marzok, B. Deh, Ph.W. Courteille, C. Zimmermann, Phys. Rev. Lett. **95**, 170408 (2005)
19. J.M. McNamara, T. Jeltes, A.S. Tychkov, W. Hogervorst, W. Vassen, Phys. Rev. Lett. **97**, 080404 (2006)
20. T. Fukuhara, Y. Takasu, S. Sugawa, Y. Takahashi, J. Low. Temp. Phys. **148**, 441 (2007)
21. H.P. Büchler, G. Blatter, Phys. Rev. Lett. **91**, 130404 (2003)
22. S. Sachdev, Nat. Phys. Physics **4**, 173 (2008)
23. R. Roth, K. Burnett, Phys. Rev. A **69**, 021601(R) (2004)

24. K. Góral, L. Santos, M. Lewenstein, Phys. Rev. Lett. **88**, 170406 (2002)
25. V. Ahufnger, L. Sanchez-Palencia, A. Kantian, A. Sanpera, M. Lewenstein, Phys. Rev. A **72**, 063616 (2005)
26. H.P. Büchler, G. Blatter, Phys. Rev. A **69**, 063603 (2004)
27. V.W. Scarola, S. Das Sarma, Phys. Rev. Lett. **95**, 033003 (2005)
28. F. Hébert, G.G. Batrouni, X. Roy, V.G. Rousseau, Phys. Rev. B **78**, 184505 (2008)
29. S. Tewari, R.M. Lutchyn, S. Das Sarma, Phys. Rev. B **80**, 054511 (2009)
30. T. Mishra, R.V. Pai, S. Ramanan, M.S. Luthra, B.P. Das, Phys. Rev. A **80**, 043614 (2009)
31. L.-M. Duan, E. Demler, M.D. Lukin, Phys. Rev. Lett. **91**, 090402 (2003)
32. C. Zhang, V.W. Scarola, S. Das Sarma, Phys. Rev. A **76**, 023605 (2007)
33. M. Maik, P. Hauke, O. Dutta, J. Zakrzewski, M. Lewenstein, New. J. Phys. **14**, 113006 (2012)
34. J. Stuhler, A. Griesmaier, T. Koch, M. Fattori, T. Pfau, S. Giovanazzi, P. Pedri, L. Santos, Phys. Rev. Lett. **95**, 150406 (2005)
35. M. Lu, S.H. Youn, B.L. Lev, Phys. Rev. Lett. **104**, 063001 (2010)
36. G. Igel-Mann, U. Wedig, P. Fuentealba, H. Stoll, J. Chem. Phys. **84**, 5007 (1986)
37. C. Menotti, M. Lewensteint, T. Lahaye, T. Pfau, AIP Conf. Proc. **970**, Conferene at Assisi, Italy, 4–8 July (2007). Also at arXiv:0711:3422v1
38. A. Griesmaier, J. Stuhler, T. Koch, M. Fattori, T. Pfau, S. Giovanazzi, Phys. Rev. Lett. **97**, 250402 (2006)
39. D. Tong, S.M. Farooqi, J. Stanojevic, S. Krishnan, Y.P. Zhang, R. Côté, E.E. Eyler, P.L. Gould, Phys. Rev. Lett. **93**, 063001 (2004)
40. D. Bohm, D. Pines, Phys. Rev. **92**, 609 (1953)
41. F. Dalfovo, S. Giorgini, L.P. Pitaevskii, S. Stringari, Rev. Mov. Phys. **71**, 463 (1999)
42. L. Viverit , S. Giorgini, Phys. Rev. A **66**, 063604 (2002)
43. D.H. Santamore, E. Timmermans, Phys. Rev. A **78**, 013619 (2008)
44. C. Cohen-Tannoudji, B. Diu, F. Laloe, *Quantum Mechanics*, Vol. 2, Chap. XI (Wiley-Interscience, New York, 1977)
45. J.H. Van Vleck, Rev. Mod. Phys. **34**, 681 (1962)
46. J. Friedel, Nuovo Cimento Suppl. **7**, 287 (1958)
47. G.E. Simion, G.E. Giuliani, Phys. Rev. B **72**, 045127 (2005)
48. M.A. Ruderman, C. Kittel, Phys. Rev. **96**, 99 (1945)
49. T. Kasuya, Prog. Theor. Phys. **16**, 45 (1956)
50. K. Yosida, Phys. Rev. **106**, 893 (1957)
51. P. Bruno, C. Chappert, Phys. Rev. Lett. **67**, 1602 (1991)
52. P. Bruno, C. Chappert, Phys. Rev. B **46**, 261 (1992)
53. A. Akbari, I. Eremin, P. Thalmeier, Phys. Rev. B **84**, 134513 (2011)
54. J. Lindhard, Kgl. Danske Videnskab. Selkab Mat. Fys. Medd. **28** (8) (1954)
55. K.-K. Ni, S. Ospelkaus, M.H.G. de Miranda, A. Pe'er, B. Neyenhuis, J.J. Zirbel, S. Kotochigova, P.S. Julienne, D.S. Jin, J. Ye, Science **322**, 231 (2008)
56. V. Bendkowsky, B. Butscher, J. Nipper, J.P. Shaffer, R. Löw, T. Pfau, Nature **458**, 1005 (2009)
57. A. Griesmaier, J. Werner, S. Hensler, J. Stuhler, T. Pfau, Phys. Rev. Lett. **94**, 160401 (2005)
58. D.M. Stamper-Kurn, J.H. Thywissen, e-print: arXiv:1111.6196v1 (2011)
59. P.O. Fedichev, M.W. Reynolds, G.V. Shlyapnikov, Phys. Rev. Lett. **77**, 2921 (1996)
60. P.F. Bedaque, Eric Braaten, H.-W. Hammer, Phys. Rev. Lett. **85**, 908 (2000)
61. H. Suno, B.D. Esry, Phys. Rev. A **80**, 062702 (2009)
62. K. Sheshadri, H.R. Krishnamurthy, R. Pandit, T.V. Ramakrishnan, Europhys. Lett. **22**, 257 (1993)
63. D. van Oosten, P. van der Straten, H.T.C. Stoof, Phys. Rev. A **63**, 053601 (2001)
64. V. Venturi, M.J. Jamieson, R. Côté, J. Phys. B At. Mol. Opt. Phys. **34**, 4339 (2001)
65. E.R.I. Abraham, W.I. McAlexander, J.M. Gerton, R.G. Hulet, R. Côté, A. Dalgarno, Phys. Rev. A **55**, 3299(R) (1997)
66. C.-H. Wu, I. Santiago, J.W. Park, P. Ahmadi, M.W. Zwierlein, Phys. Rev. A **84**, 011601(R) (2011)
67. S. Inouye, J. Goldwin, M.L. Olsen, C. Ticknor, J.L. Bohn, D.S. Jin, Phys. Rev. Lett. **93**, 183201 (2004)
68. C.A. Stan, M.W. Zwierlein, C.H. Schunck, S.M.F. Raupach, W. Ketterle, Phys. Rev. Lett. **93**, 143001 (2004)
69. M.S. Safronova, B. Arora, C.W. Clark, Phys. Rev. A **73**, 022505 (2005)
70. B. Deh, C. Marzok, C. Zimmermann, Ph.W. Courteille, Phys. Rev. A **77**, 010701(R) (2008)
71. A. Marte, T. Volz, J. Schuster, S. Dürr, G. Rempe, E.G.M. van Kempen, B.J. Verhaar, Phys. Rev. Lett. **89**, 283202 (2002)
72. J. Söding, D. Guéry-Odelin, P. Desbiolles, F. Chevy, H. Inamori, J. Dalibard, Appl. Phys. B. **69**, 257 (1999)
73. B.D. Esry, C.H. Greene, J.P. Burke, Phys. Rev. Lett. **83**, 1751 (1999)
74. D. Jaksch, C. Bruder, J.I. Cirac, C.W. Gardiner, P. Zoller, Phys. Rev. Lett. **81**, 3108 (1998)
75. P.B. Blakie, J.V. Porto, Phys. Rev. A **69**, 013603 (2004)
76. P. Sengupta, L.P. Pryadko, F. Alet, M. Troyer, G. Schmid, Phys. Rev. Lett. **94**, 207202 (2005)
77. V.W. Scarola, E. Demler, S. Das Sarma, Phys. Rev. A **73**, 051601(R) (2006)
78. A. Friedenauer, H. Schmitz, J.T. Glueckert, D. Porras, T. Schaetz, Nat. Phys. **4**, 757 (2008)
79. S. Trotzky, P. Cheinet, S. Flling, M. Feld, U. Schnorrberger, A.M. Rey, A. Polkovnikov, E.A. Demler, M.D. Lukin, I. Bloch. Science **319**, 295 (2007)
80. J. Simon, W.S. Bakr, R. Ma, M.E. Tai, P.M. Preiss, M. Greiner, Nature **472**, 307 (2011)
81. D.P. Arovas, A. Auerbach, Phys. Rev. B **38**, 316 (1988)